New Journal of Physics
The open access journal at the forefront of physics

Deutsche Physikalische Gesellschaft DPG IOP Institute of Physics

PAPER • OPEN ACCESS

Noise spectrum of a quantum dot–resonator lasing circuit

To cite this article: Jinshuang Jin *et al* 2013 *New J. Phys.* **15** 025044

New Journal of Physics
The open access journal for physics

Noise spectrum of a quantum dot–resonator lasing circuit

Jinshuang Jin[1,2], Michael Marthaler[1], Pei-Qing Jin[1,3], Dmitry Golubev[4] and Gerd Schön[1,4,5,6]

[1] Institut für Theoretische Festkörperphysik, Karlsruhe Institute of Technology, D-76128 Karlsruhe, Germany
[2] Department of Physics, Hangzhou Normal University, Hangzhou 310036, People's Republic of China
[3] Institute of Logistics Engineering, Shanghai Maritime University, Shanghai 201306, People's Republic of China
[4] Institute für Nanotechnologie, Karlsruhe Institute of Technology, D-76021 Karlsruhe, Germany
[5] DFG Center for Functional Nanostructures, Karlsruhe Institute of Technology, D-76128 Karlsruhe, Germany
E-mail: schoen@kit.edu

New Journal of Physics **15** (2013) 025044 (15pp)
Received 8 November 2012
Published 28 February 2013
Online at http://www.njp.org/
doi:10.1088/1367-2630/15/2/025044

Abstract. Single-electron tunneling processes through a double quantum dot can induce a lasing state in an electromagnetic resonator which is coupled coherently to the dot system. Here we study the noise properties of the transport current in the lasing regime, i.e. both the zero-frequency shot noise and the noise spectrum. The former shows a remarkable super-Poissonian behavior when the system approaches the lasing transition, but a sub-Poissonian behavior deep in the lasing state. The noise spectrum contains information about the coherent dynamics of the coupled dot–resonator system. It shows pronounced structures at frequencies matching that of the resonator due to the excitation of photons. For strong interdot Coulomb interaction, we observe asymmetries in the auto-correlation noise spectra of the left and right junctions, which we trace back to asymmetries in the incoherent tunneling channels.

[6] Author to whom any correspondence should be addressed.

Contents

1. Introduction

A variety of fundamental quantum effects and phenomena characteristic for cavity quantum electrodynamics (QED) has been demonstrated in superconducting circuit QED [1–4]. The equivalent of single-atom lasing has been observed, with frequencies in the few GHz range, when a single Josephson charge qubit is strongly coupled to a superconducting transmission line resonator [5, 6]. This progress stimulated the study of a different circuit QED setup where the superconducting qubit is replaced by a semiconductor double quantum dot with discrete charge states. Incoherent single-electron tunneling through the double dot sandwiched between two electrodes can lead to a population inversion in the dot levels and, as a consequence, induce a lasing state in the resonator [7, 8]. The potential advantages of quantum dots are their high tunability, both of the couplings and energy levels [9–11]. In addition, larger frequencies are accessible since the restriction to frequencies below the superconducting gap is no longer needed. Experimental progress has recently been made in coupling semiconductor quantum dots to a GHz-frequency high-quality transmission line resonator [12–14].

The double quantum dot–resonator circuit lasing setup differs from the more familiar interband transition semiconductor laser [15, 16], where the cavity mode is coupled to the lowest quantum dot interband transition, and which is driven by carrier injection in a p–n-junction or via optical pumping. Since the circuit considered here is driven by single-electron tunneling, the lasing state correlates with electron transport properties. This fact allows probing the former via a current measurement [8]. Further information about the system is contained in the current fluctuations. Due to the charge discreteness the noise is shot noise, which has been studied extensively [17–23]. For the double dot–resonator lasing circuit, it is therefore important to compare the electron shot noise with the fluctuations of the photons in the resonator.

Although more difficult, experimental progress has also been made toward measuring the finite-frequency noise spectrum of electron transport [24]. It contains information about the full dynamics of the system, including the relevant time scales that characterize the transport processes. In this work, we therefore investigate the frequency-dependent noise spectrum of the transport current through the system in and near the lasing regime. It shows pronounced

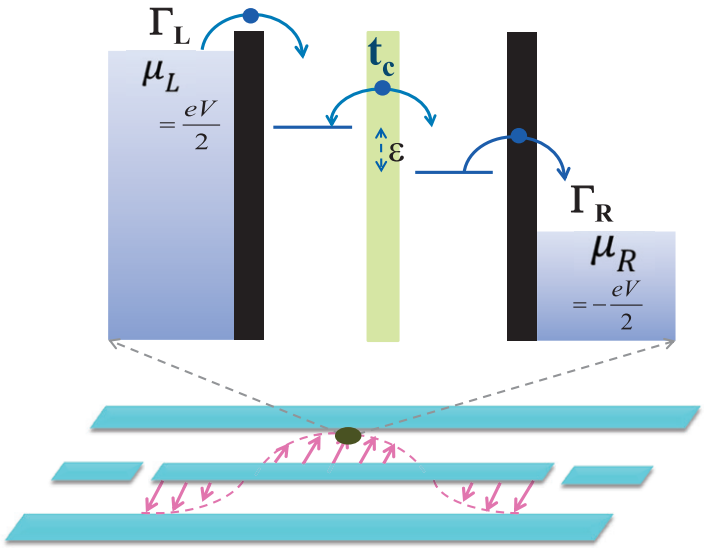

Figure 1. A double quantum dot–resonator lasing circuit. The dot is placed at a maximum of the electric field of the transmission line in order to maximize the dipole interaction. The population inversion in the dot levels, leading to the lasing state, is created by incoherent electron tunneling through the dots, driven by the bias voltage, which is assumed to be high, $eV = \mu_L - \mu_R \gg \omega_r$.

characteristic signals at frequencies close to the eigen-Rabi frequency of the coupled system or matching that of the resonator.

This paper is organized as follows. In section 2, we introduce the model of a quantum dot–resonator lasing circuit and the methods. We extend the work of [8], where strong interdot Coulomb interaction was assumed, to arbitrary strength interaction [25]. The method used for the calculation of the noise spectrum is based on a master equation combined with the quantum regression theorem. In section 3, the stationary properties of the resonator, the average current and the zero-frequency noise are studied. The finite-frequency noise spectrum is evaluated in section 4 in the low- and high-frequency regimes, both for strong and weak interdot Coulomb interaction. We find characteristic symmetric and asymmetric features in the frequency-dependent noise spectrum. We conclude with a discussion in section 5.

2. Methodology

2.1. The model

We consider the electron transport setup schematically shown in figure 1, where electrons tunnel through a semiconducting double quantum dot coupled to a high-Q electromagnetic resonator such as a superconducting transmission line. The Hamiltonian includes the interacting dot–resonator system, $H_S = H_d + H_r + H_I$, which is responsible for the coherent dynamics. The double dot is described by

$$H_d = \sum_j \varepsilon_j d_j^\dagger d_j + U d_l^\dagger d_l d_r^\dagger d_r + \frac{t_c}{2}(d_l^\dagger d_r + d_r^\dagger d_l) \tag{1}$$

with $d_j^\dagger$ being the electron creation operators for the two levels in the dots j ($j = \mathrm{l}, \mathrm{r}$) with energies ε_j, separated by $\varepsilon = \varepsilon_\mathrm{l} - \varepsilon_\mathrm{r}$, which are coupled coherently with strength t_c. Both ε_j and t_c can be tuned by gate voltages [10, 11, 26–28]. The interdot Coulomb interaction is denoted by U. The transmission line can be modeled as a harmonic oscillator, $H_\mathrm{r} = \omega_\mathrm{r} a^\dagger a$, with frequency ω_r and $a^\dagger$ denoting the creation operator of photons in the resonator. The dipole moment induces an interaction between the resonator and the double dot, H_I, which will be specified below.

We further account for electron tunneling between the dots and electrodes, $H_\mathrm{t} = \sum_k (V_{\mathrm{L}k} c_{Lk}^\dagger d_\mathrm{l} + V_{\mathrm{R}k} c_{Rk}^\dagger d_\mathrm{r} + \mathrm{H.c.})$, with tunneling amplitudes $V_{\alpha k}$ (with $\alpha = \mathrm{L}, \mathrm{R}$). The electrodes with $H_\mathrm{b} = \sum_{\alpha k} \varepsilon_{\alpha k} c_{\alpha k}^\dagger c_{\alpha k}$ act as baths. Here $c_{\alpha k}^\dagger$ is the electron creation operator for an electron state in the electrode α. Below, the tunneling between the electrodes and the dots is assumed to be an incoherent process.

The double dot can be biased such that at most one electron occupies each dot. The two charge states $|L\rangle$ and $|R\rangle$ serve as the basis of a charge qubit [29, 30]. In this work, we consider two limits, (i) strong U and (ii) weak U, respectively. In case (i), transport through the double dots involves only one extra third state, namely the empty dot $|0\rangle$, whereas in case (ii), two extra states, $|0\rangle$ and the double occupation state $|2\rangle \equiv |LR\rangle$, are involved in the transport. In both limits the dipole interaction between the resonator and the double dot is $H_\mathrm{I} = \hbar g_0 (a^\dagger + a)\tau_z$, with Pauli matrices acting in the space of the two charge states, $\tau_z = |L\rangle\langle L| - |R\rangle\langle R|$.

In the eigenbasis of the double dot and within rotating wave approximation, the Hamiltonian of the coupled dot–resonator system, for strong interdot Coulomb interaction, can be reduced to

$$H_\mathrm{S} = \frac{\hbar\omega_0}{2}\sigma_z + \hbar\omega_\mathrm{r} a^\dagger a + \hbar g(a^\dagger \sigma_- + a\sigma_+), \tag{2}$$

while for weak interdot interaction an extra term $U|2\rangle\langle 2|$ is to be included. In the restricted space of states we have $d_\mathrm{l} = |0\rangle\langle L| + |R\rangle\langle 2|$ and $d_\mathrm{r} = |0\rangle\langle R| - |L\rangle\langle 2|$, and the Pauli matrix operates in the eigenbasis, i.e. $\sigma_z = |e\rangle\langle e| - |g\rangle\langle g|$ with

$$\begin{aligned} |e\rangle &= \cos(\theta/2)\,|L\rangle + \sin(\theta/2)\,|R\rangle, \\ |g\rangle &= \sin(\theta/2)\,|L\rangle - \cos(\theta/2)\,|R\rangle. \end{aligned} \tag{3}$$

Here, we fix the zero energy level by $\varepsilon_\mathrm{l} + \varepsilon_\mathrm{r} = 0$. The angle $\theta = \arctan(t_\mathrm{c}/\varepsilon)$ characterizes the mixture of the pure charge states, the coupling strength is $g = g_0 \sin\theta$ and $\omega_0 = \sqrt{\varepsilon^2 + t_c^2}/\hbar$ denotes the level spacing of the two eigenstates. It can be tuned via gate voltages, which allows control of the detuning $\Delta = \omega_0 - \omega_\mathrm{r}$ from the resonator frequency.

2.2. Master equation

The dynamics of the coupled dot–resonator system, which is assumed to be weakly coupled to the electron reservoirs with smooth spectral density, can be described by a master equation for the reduced density matrix ρ in the Born–Markov approximation [31, 32]. Throughout this paper, we consider low temperatures, $T = 0$, with vanishing thermal photon number and excitation rates. Consequently, the master equation is

$$\dot\rho = -\frac{\mathrm{i}}{\hbar}[H_\mathrm{S}, \rho] + \mathcal{L}_\mathrm{L}\,\rho + \mathcal{L}_\mathrm{R}\,\rho + \mathcal{L}_\mathrm{r}\,\rho \equiv \mathcal{L}_\mathrm{tot}\,\rho, \tag{4a}$$

where the dissipative dynamics is described by Lindblad operators of the form

$$\mathcal{L}_i \rho = \frac{\Gamma_i}{2}(2L_i \rho L_i^\dagger - L_i^\dagger L_i \rho - \rho L_i^\dagger L_i). \tag{4b}$$

The first two terms $\mathcal{L}_{\rm L/R}$ account for the incoherent sequential tunneling between the electrodes and the dots with $\Gamma_\alpha(\omega) = 2\pi \sum_k |V_{\alpha k}|^2 \delta(\omega - \varepsilon_{\alpha k}) \equiv \Gamma_\alpha$. For the assumed high voltage and low temperature, i.e. in the absence of reverse tunneling processes, we have $L_{\rm L} = d_{\rm l}^\dagger$ and $L_{\rm R} = d_{\rm r}$ with tunneling rates $\Gamma_{\rm L}$ and $\Gamma_{\rm R}$, respectively. For the oscillator we take the standard decay term $L_{\rm r} = a$ with rate $\Gamma_{\rm r} = \kappa$. Here, we ignore other dissipative effects, such as relaxation and dephasing of the two charge states, which were studied in [8], since such effects only weakly affect the main points we wish to study.

From the definition $I_\alpha(t) \equiv -e\frac{{\rm d}\langle n_\alpha(t)\rangle}{{\rm d}t}$ with $n_\alpha = \sum_k c_{\alpha k}^\dagger c_{\alpha k}$, it is straightforward to obtain the transport current from the electrodes to the dots [33, 34], $I_\alpha(t) = {\rm Tr}[\hat{I}_\alpha \rho(t)]$, with current operators given by

$$\hat{I}_{\rm L}\rho(t) = \frac{e}{\hbar}\Gamma_{\rm L} d_{\rm l}^\dagger \rho(t) d_{\rm l}, \tag{5a}$$

$$\hat{I}_{\rm R}\rho(t) = -\frac{e}{\hbar}\Gamma_{\rm R} d_{\rm r} \rho(t) d_{\rm r}^\dagger. \tag{5b}$$

In the stationary limit, $t \to \infty$, the average current satisfies $I = \frac{1}{2}(I_{\rm L} - I_{\rm R}) = I_{\rm L} = -I_{\rm R}$, consistent with charge conservation.

2.3. Current noise spectrum

We consider the symmetrized current noise spectrum

$$\begin{aligned} S(\omega) &= \mathcal{F}\langle\{\delta\hat{I}(t), \delta\hat{I}(0)\}\rangle \\ &\equiv \int_{-\infty}^{\infty} {\rm d}t\, {\rm e}^{{\rm i}\omega t}\langle\{\delta\hat{I}(t), \delta\hat{I}(0)\}\rangle \\ &= 2\,{\rm Re}\{\widetilde{G}_I(\omega) + \widetilde{G}_I(-\omega)\}, \end{aligned} \tag{6}$$

where $\delta\hat{I}(t) = \hat{I}(t) - I$ and $\widetilde{G}_I(\pm\omega) = \int_0^\infty {\rm d}t\, {\rm e}^{\pm{\rm i}\omega t} G_I(t)$ with $G_I(t) = \langle\delta\hat{I}(t)\delta\hat{I}(0)\rangle$. In the Born–Markov approximation, the current noise spectrum can be calculated via the widely used MacDonald's formula [35] or the quantum regression theorem [31]. Since we already know the current operators, as expressed in equation (5), it is more convenient to calculate the current correlation function via the quantum regression theorem

$$G_I(t) = {\rm Tr}\big[\hat{I}\,{\rm e}^{\mathcal{L}_{\rm tot}t}\hat{I}\rho^{\rm st}\big] - I^2, \tag{7}$$

where $\rho^{\rm st}$ denotes the steady-state density matrix.

According to the Ramo–Shockley theorem, the measured quantity in most experiments [19] is the total circuit current $I(t) = aI_{\rm L}(t) - bI_{\rm R}(t)$, with coefficients, $a + b = 1$, depending on the symmetry of the transport setup (e.g. the junction capacitances). The circuit noise spectrum is thus composed of three components: $S(\omega) = a^2 S_{\rm L}(\omega) + b^2 S_{\rm R}(\omega) - 2ab S_{\rm LR}(\omega)$ [19, 36], where $S_\alpha(\omega) = \mathcal{F}\langle\{\delta\hat{I}_\alpha(t), \delta\hat{I}_\alpha(0)\}\rangle$ are the auto-correlation noise spectra of the current from lead-α, and $S_{\rm LR}(\omega) = (\mathcal{F}\langle\{\delta\hat{I}_{\rm L}(t), \delta\hat{I}_{\rm R}(0)\}\rangle + \mathcal{F}\langle\{\delta\hat{I}_{\rm L}(t), \delta\hat{I}_{\rm R}(0)\}\rangle)/2$ is the current cross-correlation noise spectrum between different leads. Alternatively, in view of the charge conservation, i.e. $I_{\rm L} = I_{\rm R} + {\rm d}Q/{\rm d}t$, where Q is the charge on the central dots, the circuit noise spectrum can be expressed as [37–39] $S(\omega) = aS_{\rm L}(\omega) + bS_{\rm R}(\omega) - ab\,S_{\rm C}(\omega)$ with $S_{\rm C}(\omega) \equiv \mathcal{F}\langle\{\delta\dot{Q}(t), \delta\dot{Q}(0)\}\rangle = 2S_{\rm LR}(\omega) + S_{\rm L}(\omega) + S_{\rm R}(\omega)$ [40]. Thus, from the behavior of the auto-correlation and cross-correlation noise spectra, which will be studied in the following, we can fully understand the

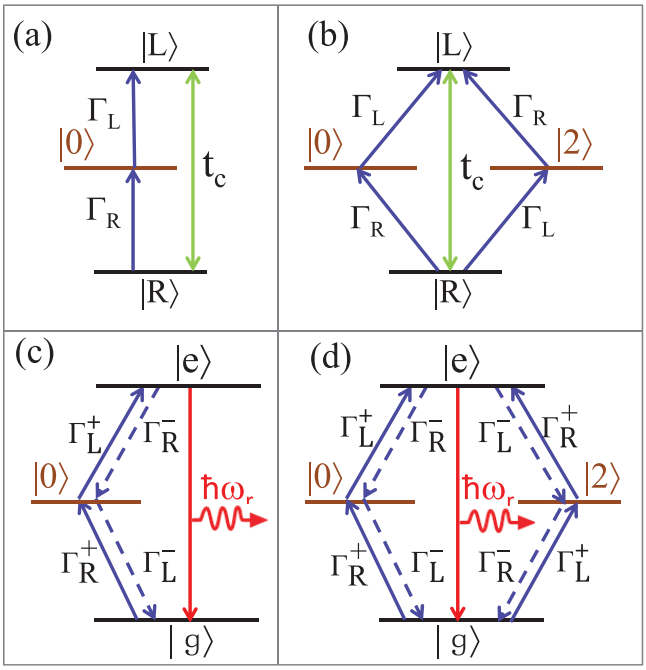

Figure 2. Incoherent electron tunneling induces transitions between different states in the dot. The upper panels, (a) and (b), and the lower ones, (c) and (d), describe the incoherent transitions in the dot-basis and eigenbasis (including the interaction with the resonator), respectively. Panels (a) and (c) correspond to asymmetric transition channels for strong interdot Coulomb interaction, and panels (b) and (d) to symmetric transition channels for weak interdot Coulomb interaction. Furthermore, we have $\Gamma_\alpha^+ = \Gamma_\alpha \cos^2(\theta/2)$ and $\Gamma_\alpha^- = \Gamma_\alpha \sin^2(\theta/2)$ with $\alpha = \mathrm{L}, \mathrm{R}$.

circuit noise spectrum even including the charge fluctuation spectrum in the central dots, $S_\mathrm{C}(\omega)$. At zero frequency, we have $S(0) = S_\mathrm{L}(0) = S_\mathrm{R}(0) = -S_\mathrm{LR}(0)$ and $S_\mathrm{C}(0) = 0$ due to current conservation in the steady state.

3. Stationary properties

Let us first recall the parameter regime for which, according to [8], lasing can be induced for the present setup [12–14]. We consider the level spacing in the dots comparable to the resonator frequency ω_r in the range of a few GHZ, and a high-quality resonator with Q factor assumed to be 5×10^4, corresponding to a decay rate $\kappa = 2 \times 10^{-5}\omega_\mathrm{r}$. The coupling of the dot and the resonator, chosen as $g_0 = 10^{-3}\omega_\mathrm{r}$, is strong enough compared to the photon decay rate in the resonator, and we assume weak incoherent tunneling with $\Gamma_\mathrm{L} = \Gamma_\mathrm{R} = \Gamma = 10^{-3}\omega_\mathrm{r}$ to be a few MHz throughout the paper, unless otherwise stated.

A crucial prerequisite for lasing is a pumping mechanism [5, 41], involving a third state, which creates a population inversion in the two-level system. In [8], the empty state $|0\rangle$ in the double dot was considered as the single third state under the assumption of strong charging energy, $\varepsilon_j + U > \mu_\mathrm{L} > \varepsilon_j > \mu_\mathrm{R}$. This limit, which we call case (i), is sketched in figure 2(a). On the other hand, the interdot Coulomb interaction may also be weaker compared to the level

spacing of the charge states. In the tunneling regime, we have $\mu_L > \varepsilon_j, \varepsilon_j + U > \mu_R$. This limit, called case (ii), where two extra states are involved in the incoherent tunneling, is illustrated in figure 2(b). The question arises, which case is better for lasing.

Let us first consider the key factor for lasing, i.e. the population inversion defined by $\tau_0 = (\rho_e^{st} - \rho_g^{st})/(\rho_e^{st} + \rho_g^{st})$, with $\rho_i^{st} = \sum_n \langle i, n|\rho^{st}|i, n\rangle$ being the stationary population of the state of the dots ($i = e, g$). Explicitly, we find that

$$\tau_0 = \begin{cases} \dfrac{(\Gamma_R^2/\omega_0^2 + 4)\cos\theta}{\Gamma_R^2/\omega_0^2 + 3 + \cos 2\theta} & \text{for case (i),} \\ \dfrac{(\Gamma_0^2/\omega_0^2 + 4)\cos\theta}{\Gamma_0^2/\omega_0^2 + 3 + \cos 2\theta} & \text{for case (ii)} \end{cases} \tag{8}$$

with $\Gamma_0 = \Gamma_L + \Gamma_R$. The population inversion does not depend on Γ_L for case (i). But it depends on both tunneling rates for case (ii), suggesting that in this case the population inversion is driven by transitions from $|R\rangle$ to both extra states $|0\rangle$ and $|2\rangle$. See figures 2(a) and (b) for cases (i) and (ii), respectively. Although, in general, an additional incoherent tunneling channel reduces the population inversion slightly, for the parameters studied in the present work, i.e. $\Gamma \ll \omega_r$, it approaches the same value for both cases (i) and (ii), $\tau_0 \approx 4\cos\theta/(3 + \cos 2\theta)$, which reaches a maximum, $\tau_0 \to 1$, for $\theta \to \pi/2$. To balance the effective dot–resonator coupling $g = g_0 \sin\theta$ and the population inversion τ_0, following the consideration in [8], we set the interdot coupling strength $t_c = 0.3\omega_r$ throughout this work.

The properties of the resonator can be characterized by the average number of photons $\langle n\rangle$ and the Fano factor $F_n \equiv (\langle n^2\rangle - \langle n\rangle^2)/\langle n\rangle^2$ describing their fluctuations [16]. When reducing the detuning between the dot and the resonator from large values to zero, we observe that the system undergoes a transition from the nonlasing regime, where $\langle n\rangle < 1$ and $F_n = \langle n\rangle + 1$, to a lasing state with a sharp increase in the photon number. Before we reach the lasing state the photon number distribution has a thermal shape, which explains the value of the Fano factor. At the transition to the lasing regime the amplitude fluctuations lead to a peak in the Fano factor, as shown in figure 3(b). In the lasing state the photon number is saturated, and the Fano factor drops to $F_n < 1$, indicating a squeezed photon number distribution in the resonator. Interestingly, the average photon number in the lasing regime, as well as the corresponding peak in the Fano factor at the lasing transition are larger for weak interdot interaction, case (ii), than for strong one, case (i). Approximately, we obtain the average photon number [42] for case (ii)

$$\langle n\rangle \simeq \frac{\Gamma\cos\theta}{2\kappa} - \frac{\Gamma^2 + 4\Delta^2}{8g^2}. \tag{9}$$

Compared to case (i), where [8] $\langle n\rangle_i \simeq \frac{\Gamma\cos\theta}{3\kappa} - \frac{\Gamma^2+4\Delta^2}{96g^2}(7 + \cos\theta)$, we find an increase to $\langle n\rangle_{ii} \approx \langle n\rangle_i + \frac{\Gamma}{6\kappa}$, showing that case (ii) with four levels is more suited for lasing. The difference is due to the existence of one more incoherent tunneling channel, driven as illustrated in figures 2(b) and (d).

Since photons in the resonator are excited by the incoherent tunneling between the dot and the electrodes, the lasing state closely correlates with the transport current. The current can be expressed approximately (for $\kappa \ll \Gamma$ and small θ) for case (i) as [8]

$$I(\Delta) \simeq e\Gamma \sum_{n=0} P(n) \frac{(n+1)}{3(n+1) + (\Gamma^2 + 4\Delta^2)/4g^2} \tag{10}$$

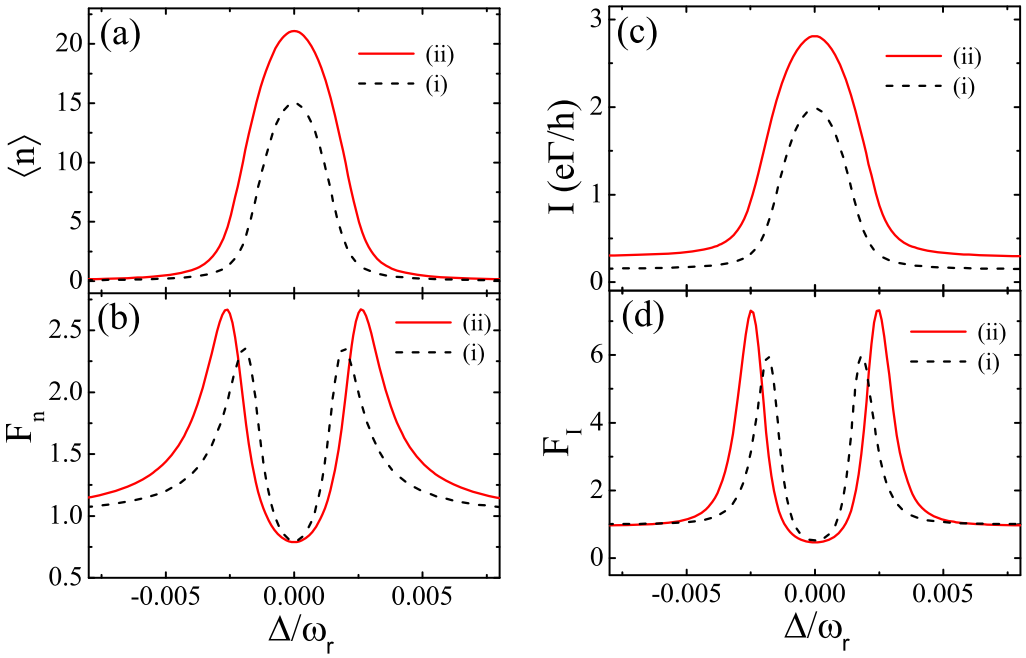

Figure 3. (a) Average photon number $\langle n\rangle$, (b) Fano factor $F_n = (\langle n^2\rangle - \langle n\rangle^2)/\langle n\rangle^2$ of photons in the resonator, (c) average current I and (d) Fano factor of the current $F_I = S(0)/2I$, as a function of detuning for weak Coulomb interaction (red solid line) and strong interaction (black dashed line). Throughout this paper, we choose the tunneling rate $\Gamma = 10^{-3}\omega_r$ and interdot coupling strength $t_c = 0.3\omega_r$.

with $P(n) \simeq (\Gamma/\kappa)P(0)\prod_{l=1}^{n}[3l + (\Gamma^2 + 4\Delta^2)/4g^2]^{-1}$ being the probability of n photons in the resonator (in [8] a factor $\frac{1}{2}$ was missing). As shown in figure 3(c), the transport current as function of the detuning follows closely the behavior of the average photon number. Similarly, the corresponding transport current for case (ii) is obtained as

$$I(\Delta) \simeq e\Gamma \sum_{n=0} P(n)\frac{(n+1)}{2(n+1) + (\Gamma^2 + 4\Delta^2)/4g^2}, \tag{11}$$

where $P(n) \simeq (\Gamma/\kappa)P(0)\prod_{l=1}^{n}[2l + (\Gamma^2 + 4\Delta^2)/4g^2]^{-1}$. Both the average photon number of the resonator and the current for case (ii) are larger than those for case (i).

As had been pointed out in [43], for a superconducting single-electron transistor (SSET) coupled to a resonator, the noise spectra of the fluctuations of the photons are correlated with the zero-frequency shot noise of the current. This fact is illustrated for the Fano factor $F_I = S(0)/2I$ in figure 3(d). For strong detuning in the nonlasing regime, where the dots effectively do not interact with the resonator, the shot noise shows a Poissonian distribution, i.e. $F_I \simeq 1$. Near the lasing transition the shot noise is enhanced strongly with a super-Poissonian distribution. Compared to the Fano factor of the photons, the signal in the shot noise is stronger with a narrower transition window and sharper peak. In the lasing state, where the photons are saturated and the transport current reaches the maximum value, we find sub-Poissonian current noise, $F_I \simeq 0.5$, while the photon Fano factor F_n describes a squeezed state of the radiation field in this nonclassical regime, differing from a conventional coherent state with Poissonian distribution.

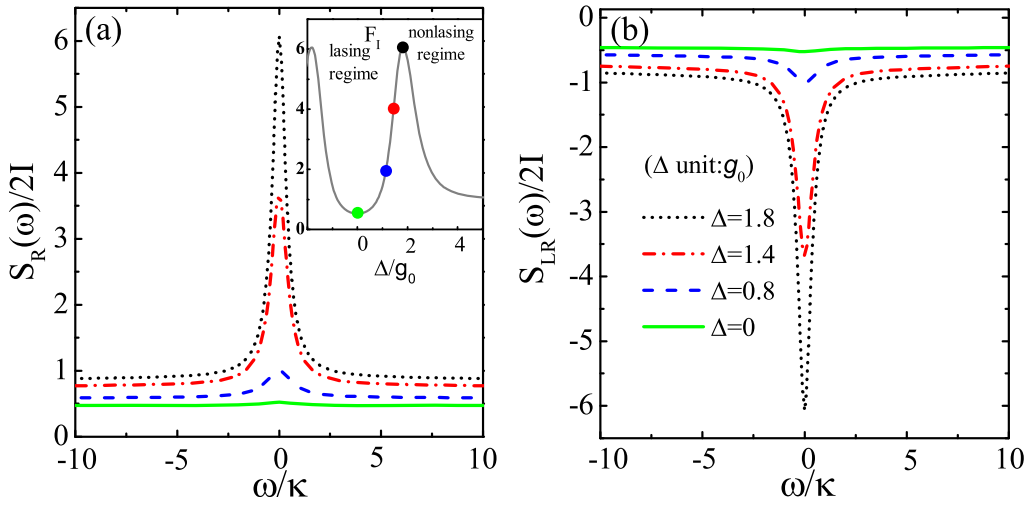

Figure 4. The noise spectra in the low-frequency regime for strong interdot Coulomb interaction. (a) Auto-correlation $S_L(\omega) = S_R(\omega)$. (b) Cross-correlation $S_{LR}(\omega)$. Different colors of the plotted noise spectra refer to different values of the detuning, as denoted in the inset of (a) by color circles. The other parameters are the same as in figure 3.

The cross-correlation noise (not displayed in the figures) shows a similar behavior with the opposite sign due to the relation $S_L(0) = S_R(0) = -S_{LR}(0)$.

4. Noise spectrum

Since in the nonlasing regime the noise spectrum displays only trivial features, we focus in the following on the finite-frequency noise spectra in the lasing regime and at the lasing transition, as shown in the inset of figure 4(a). For tunneling dissipative operators $\mathcal{L}_L$ and $\mathcal{L}_R$ as defined after equation (4*b*) it has been demonstrated [44] that all correlation functions can be expanded in terms of the eigenvalues λ_k of $\mathcal{L}_{tot}$ and the coefficients $c_k = [\hat{V}^{-1}\hat{I}_\alpha\hat{V}]_{kk}$. Here $\hat{V}$ is built from the eigenvectors of $\mathcal{L}_{tot}$, and $\hat{I}_\alpha$ is the current operator described in equation (5). For example, we have

$$\frac{S_\alpha(\omega)}{2I} = 1 - 2\sum_k \frac{\mathrm{Re}(c_k)\mathrm{Re}(\lambda_k) + \mathrm{Im}(c_k)[\omega + \mathrm{Im}(\lambda_k)]}{[\omega + \mathrm{Im}(\lambda_k)]^2 + [\mathrm{Re}(\lambda_k)]^2}, \tag{12}$$

where the imaginary part $\mathrm{Im}(\lambda_k)$ and the real part $\mathrm{Re}(\lambda_k)$ represent the coherent and dissipative dynamics, respectively. The coherent dynamics follows from the Jaynes–Cummings Hamiltonian, equation (2), with eigenstates [3, 45]

$$|+, n\rangle = \cos\theta_n|e, n\rangle + \sin\theta_n|g, n+1\rangle, \tag{13}$$

$$|-, n\rangle = \sin\theta_n|e, n\rangle - \cos\theta_n|g, n+1\rangle \tag{14}$$

and eigenenergies

$$E_{\pm,n} = (n+1)\omega_r \pm \frac{1}{2}\sqrt{4g^2(n+1) + \Delta^2} \tag{15}$$

with $\theta_n = \frac{1}{2}\tan^{-1}(\frac{2g\sqrt{n+1}}{\Delta})$. The typical signal in the noise spectrum is dominated by these eigenenergies, while the linewidth of the signal follows from the jump operators in equation (4*b*).

4.1. Low-frequency regime

Let us first consider the low-frequency regime around $\omega \sim 0$ displayed in figure 4. We find a zero-frequency peak and dip in the auto- and cross-correlation noise spectra, respectively. Both decrease and finally disappear when one approaches the lasing state. The height of the zero-frequency peak as a function of a detuning is shown in figure 3(d). Since in the absence of a resonator we have $S_\alpha(\omega \approx 0)/2I = -S_{\rm LR}(\omega \approx 0)/2I \simeq 1$, the peak/dip feature at zero frequency in the noise spectra must be the effect of the resonator.

The noise spectra in figure 4 have a Lorentzian shape with linewidth $\gamma_0 \sim \kappa$, determined by the emission spectrum of the photons [32]. In the regime around zero frequency, corresponding to the long-time limit, the noise spectra are determined by the single minimum eigenvalue $\lambda_{\rm min}$ with the real part dominated by the weakest decay rate, i.e. κ. For weak interdot Coulomb interaction, where we have to account for one more incoherent tunneling channel (see figures 2(b) and (d)) the low-frequency noise spectra display a similar behavior as in figure 4(d), except for the enhancement of the zero-frequency peak as shown in figure 3. It is worth noting that in this low-frequency regime, the relation $S_{\rm L}(\omega \sim 0) = S_{\rm R}(\omega \sim 0) = -S_{\rm LR}(\omega \sim 0)$ is still satisfied. However, as we will show below, the cross-correlation noise changes sign beyond the low-frequency regime.

At higher frequencies but still within the range $|\omega| < \omega_{\rm r}$, the spectra are no longer Lorentzian due to the contributions from several λ_k in equation (12). We find characteristic features showing a step and peak in the auto- and cross-correlation noise spectra, respectively, as shown in figure 5. The position of the step/peak is nearly independent of the detuning, while the magnitude is sensitive to it. With increasing dot–resonator interaction, both the step and peak are shifted as shown in figure 6. These characteristics are a consequence of the coherent dynamics of the coupled dot–resonator system. The step/peak occurs at $\omega = \delta E$, where $\delta E = |E_{+,\langle n\rangle} - E_{-,\langle n\rangle}| = \sqrt{4g^2(\langle n\rangle + 1) + \Delta^2} \approx 2g(\langle n\rangle + 1)$ is the Rabi frequency corresponding to the photon number $\langle n\rangle$. As expected, this coherent signal of the step/peak becomes weak and even disappears with increasing incoherent tunneling rate Γ (not shown in the figure). Interestingly, as shown in figure 6(b), we find that with increasing dot–resonator interaction, the coherent signal for weak interdot Coulomb interaction is not only shifted, but the step also turns into a dip. This is consistent with the coherent signal of the Rabi frequency in the double dot in the absence of the resonator showing a dip and peak in the auto- and cross-correlation noise spectra, respectively [39, 46]. It arises from the recovered symmetrical transition tunneling channels (figures 2(b) and (d)). In the low-frequency regime, $\omega < |\omega_{\rm r}|$, the auto-correlation noise spectra of left and right leads satisfy $S_{\rm L}(\omega) = S_{\rm R}(\omega)$. This is no longer true in the high-frequency regime $\omega \gtrsim |\omega_{\rm r}|$ for strong interdot Coulomb interaction, as will be shown in the following subsection.

4.2. Regime close to the resonator frequency

Before addressing the noise spectrum in the high-frequency regime, let us briefly discuss its properties in the absence of the resonator. It has been demonstrated [38, 39] that the signal of

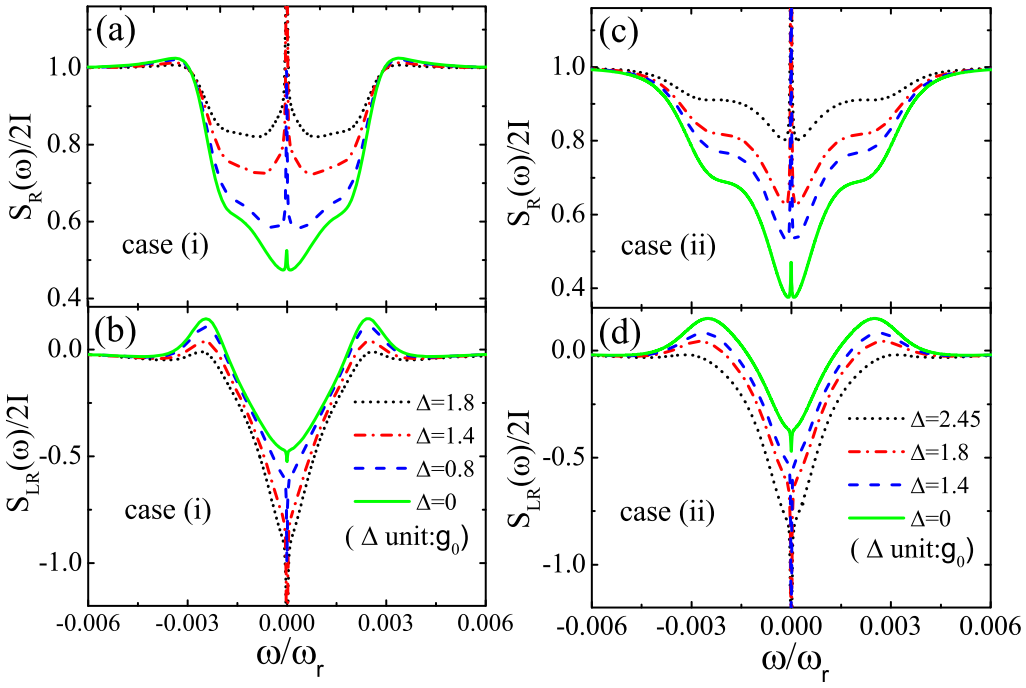

Figure 5. The low-frequency auto-correlation and cross-correlation noise spectrum for different values of the detuning in the lasing regime. Panels (a) and (b) are for strong interdot Coulomb interaction, and (c) and (d) for weak interdot Coulomb interaction. The other parameters are the same as in figure 3.

the intrinsic Rabi frequency ω_0 of the double dots can be extracted from the noise spectra. For instance, the auto-correlation noise spectrum shows a dip-peak structure and a dip at $\omega = \omega_0$ for strong and weak interdot Coulomb interactions, respectively [38, 39]. Considering the present parameter regime, where lasing is induced for $\omega_0 \approx \omega_r$ with very weak incoherent tunneling, $\Gamma = 10^{-3}\omega_0$, we find in the strong Coulomb interaction case nearly Poissonian noise in the full-frequency regime, with a small correction due to a weak coherent Rabi signal, i.e. $S_\alpha(\omega_0)/2I \sim 1 \pm 5 \times 10^{-5}$. The correction can be neglected compared to the signal induced by the coupled resonator as shown in figure 7.

The signals in the high-frequency noise spectrum arise because of transitions with the energy $E_{\pm,n} - E_{\pm,n-1} \approx \omega_r$. They depend on the detuning in the same way as the spectrum of the oscillator [47]. Namely, for positive detuning we find a signal at frequencies somewhat higher than ω_r and for negative detuning at frequencies below ω_r.

In contrast to the low-frequency case, for high frequencies the spectra of the current in the left and right junction, $S_L(\omega)$ and $S_R(\omega)$, do not have to be identical due to the overall symmetry of the circuit broken by the resonator. This feature has been demonstrated by the previous studies in [48, 49] for investigating the spectral properties of a resonator coupled to a single-electron transistor (SET) and a superconducting single-electron transistor (SSET), respectively, in the nonlasing regime. For the present studied setup in the lasing regime, in this case we find significant differences between the cases (i) and (ii) of strong and weak Coulomb interactions, as illustrated in the left and right columns of figure 7, respectively. For strong

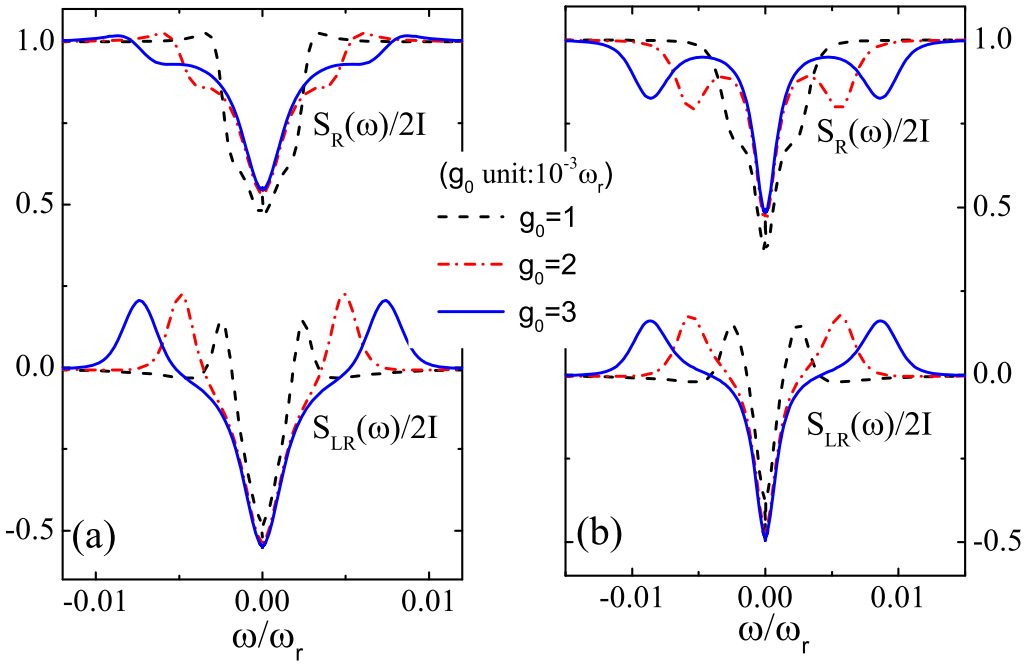

Figure 6. The low-frequency noise spectra for different dot–resonator coupling strengths in the lasing state at $\Delta = 0$: (a) for strong interdot Coulomb interactions and (b) for weak interdot Coulomb interaction. The other parameters are the same as in figure 3.

Coulomb interaction the correlators are

$$\begin{aligned}\langle I_{\rm L}(t)I_{\rm L}(0)\rangle &= \sum_n \langle n|\langle 0|\rho_{I_{\rm L}}(t)|0\rangle|n\rangle,\\ \langle I_{\rm R}(t)I_{\rm R}(0)\rangle &= \sum_n \langle n|\langle R|\rho_{I_{\rm R}}(t)|R\rangle|n\rangle,\end{aligned} \tag{16}$$

while for weak Coulomb interaction we have

$$\begin{aligned}\langle I_{\rm L}(t)I_{\rm L}(0)\rangle &= \sum_n \langle n|\left[\langle 0|\rho_{I_{\rm L}}(t)|0\rangle + \langle R|\rho_{I_{\rm L}}(t)|R\rangle\right]|n\rangle,\\ \langle I_{\rm R}(t)I_{\rm R}(0)\rangle &= \sum_n \langle n|\left[\langle R|\rho_{I_{\rm R}}(t)|R\rangle + \langle 2|\rho_{I_{\rm R}}(t)|2\rangle\right]|n\rangle.\end{aligned} \tag{17}$$

Here we introduced the density matrix $\rho_{I_i}(t)$ which satisfies the master equation (4) with the initial condition $\rho_{I_i}(0) = \hat{I}_i\rho^{\rm st}$ $(i = {\rm L}, {\rm R})$.

For strong Coulomb interaction only $S_{\rm R}(\omega)$ couples directly to the state $|R\rangle$, which in turn couples resonantly to the oscillator. As a result we observe the signal at $\omega \approx \omega_{\rm r}$ only in $S_{\rm R}(\omega)$, while $S_{\rm L}(\omega) \approx 1$ is unaffected by the oscillator. In contrast, in case (ii), where we allow the state $|2\rangle$ to participate, we again find a symmetry between the currents through the right and left junctions and $S_{\rm L}(\omega) = S_{\rm R}(\omega)$, as well as the anti-symmetry between the auto- and cross-correlation noise spectrums, i.e. roughly $S_\alpha(\omega)/2I \approx 1 + \Delta S(\omega)$ and $S_{\rm LR}(\omega)/2I \approx -\Delta S(\omega)$ with the signal $\Delta S(\omega)$ changing sign leading to a peak and a dip as function of frequency. Furthermore, in contrast to the low-frequency regime, the noise spectrum at high frequency

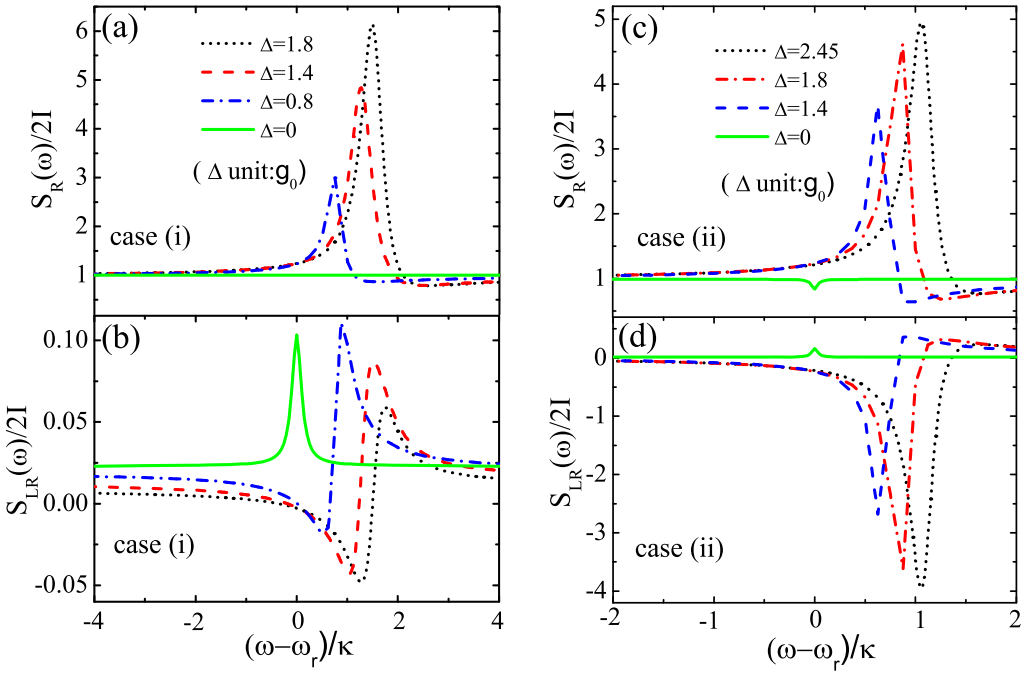

Figure 7. The finite-frequency noise spectra for strong Coulomb interaction in the lasing regime. Panels (a) and (b) are for strong interdot Coulomb interaction and panels (c) and (b) are for weak interdot Coulomb interaction. The other parameters are the same as in figure 3.

shows a Fano-resonance profile. It displays the same mechanism as observed by Rodrigues [50] that the detector (here the double quantum dot) feels the force in two ways, namely the original one from the voltage-driven tunneling and the one from the resonator. It arises from a destructive inference between the two transition paths between $|g\rangle$ and $|e\rangle$, i.e. a direct tunneling channel through the leads and a transition assisted by the absorption and emission at the detection frequency. We would like to mention that the present result differs from the observation mode in [50]. These authors found a Fano-resonance in the charge noise spectrum of a single-electron transistor coupled to a resonator and conjectured that it should also show up in other experimentally more accessible variables. We find the Fano-resonance in the current noise spectrum, which is directly observable.

5. Summary and discussion

We have evaluated the frequency-dependent noise spectrum of the transport current through a coupled dot–resonator system in the lasing regime, in a situation where incoherent tunneling induces a population inversion. We considered both strong and weak interdot Coulomb interactions, in the latter case taking into account the doubly occupied state as well. Both situations lead to a similar behavior of the zero-frequency shot noise but to different features in the finite-frequency noise spectrum.

When the system approaches the lasing regime the zero-frequency shot noise is enhanced strongly showing a remarkable super-Poissonian distribution. When the resonator is in the lasing state, the shot noise displays sub-Poissonian characteristics. The current follows here

the behavior of the photon distribution, which is also super-Poissonian as one approaches the lasing regime and becomes sub-Poissonian near resonance.

We found that the average photon number and the corresponding Fano factor, as well as the average current and its Fano factor in the lasing regime, are larger for weak interdot Coulomb interaction than for strong interaction. The zero-frequency shot noise could be detected with current experimental technologies. For example, a quantum point contact coupled to the dots has been demonstrated to detect in real-time single-electron tunneling through the double dot [22, 23].

Considering the finite-frequency noise spectra, we found pronounced characteristic structures in the low- and high-frequency regimes reflecting the coherent dynamics of the coupled dot–resonator system. At low but finite frequencies the coherent dynamics of the oscillator leads to a peak at the eigen-Rabi frequency of the coupled system. At frequencies close to that of the resonator, due to the excitations of the photons in the resonator, we found for strong interdot Coulomb interaction a strongly asymmetric signal in the auto-correlation noise spectra of the left and right junctions. Symmetry is restored for weak interdot Coulomb interaction. The difference arises from the asymmetrical and symmetrical incoherent tunneling channels induced by strong and weak interdot Coulomb interactions, respectively.

Acknowledgments

JSJ acknowledges support from the Program for Excellent Young Teachers in Hangzhou Normal University, the NSFC (10905014, 10904029 and 11274085), and the Ministry of Science, Research and the Arts of the State of Baden-Württemberg.

References

[1] Wallraff A, Schuster D I, Blais A, Frunzio L R S, Huang J M, Kumar S, Girvin S M and Schoelkopf R J 2004 *Nature* **431** 162–7
[2] Chiorescu I, Bertet P, Semba K, Nakamura Y, Harmans C J P M and Mooij J E 2004 *Nature* **431** 159–62
[3] Blais A, Huang R-S, Wallraff A, Girvin S M and Schoelkopf R J 2004 *Phys. Rev.* A **69** 062320
[4] Il'ichev E, Oukhanski N, Izmalkov A, Wagner T, Grajcar M, Meyer H-G, Smirnov A Y, Maassen van den Brink A, Amin M H S and Zagoskin A M 2003 *Phys. Rev. Lett.* **91** 097906
[5] Astafiev O, Inomata K, Niskanen A O, Yamamoto T, Pashkin Y A, Nakamura Y and Tsai J S 2007 *Nature* **448** 588–90
[6] Hauss J, Fedorov A, Hutter C, Shnirman A and Schön G 2008 *Phys. Rev. Lett.* **100** 037003
[7] Childress L, Sørensen A S and Lukin M D 2004 *Phys. Rev.* A **69** 042302
[8] Jin P-Q, Marthaler M, Cole J H, Shnirman A and Schön G 2011 *Phys. Rev.* B **84** 035322
[9] Fujisawa T, Oosterkamp T H, van der Wiel W G, Broer B W, Aguado R, Tarucha S and Kouwenhoven L P 1998 *Science* **282** 932–5
[10] Petta J R, Johnson C A, Taylor M J, Laird E A, Yacoby A, Lukin M D, Marcus C M, Hanson M P and Gossard A C 2005 *Science* **309** 2180
[11] Nowack K C, Koppens F H L, Nazarov Y V and Vandersypen L M K 2007 *Science* **318** 1430–3
[12] Frey T, Leek P J, Beck M, Blais A, Ihn T, Ensslin K and Wallraff A 2012 *Phys. Rev. Lett.* **108** 046807
[13] Frey T, Leek P J, Beck M, Ensslin K, Wallraff A and Ihn T 2011 *Appl. Phys. Lett.* **98** 262105
[14] Delbecq M R, Schmitt V, Parmentier F D, Roch N, Viennot J J, Fève G, Huard B, Mora C, Cottet A and Kontos T 2011 *Phys. Rev. Lett.* **107** 256804
[15] Benson O and Yamamoto Y 1999 *Phys. Rev.* A **59** 4756–63

[16] Strauf S and Jahnke F 2011 *Laser Photon. Rev.* **5** 607–33
[17] Hershfield S 1992 *Phys. Rev.* B **46** 7061–76
[18] Ding G-H and Ng T-K 1997 *Phys. Rev.* B **56** R15521–4
[19] Blanter Y M and Büttiker M 2000 *Phys. Rep.* **336** 1
[20] Nazarov Y V (ed) 2003 *Quantum Noise in Mesoscopic Physics* (Kluwer: Dordrecht) pp 3–31
[21] Kießlich G, Schöll E, Brandes T, Hohls F and Haug R J 2007 *Phys. Rev. Lett.* **99** 206602
[22] Gustavsson S, Leturcq R, Simovic B, Schleser R, Ihn T, Studerus P, Ensslin K, Driscoll D C and Gossard A C 2006 *Phys. Rev. Lett.* **96** 076605
[23] Fujisawa T, Hayashi T, Tomita R and Hirayama Y 2006 *Science* **312** 1634
[24] Ubbelohde N, Fricke C, Flindt C, Hohls F and Haug R J 2012 *Nature Commun.* **91** 1
[25] van der Wiel W G, De Franceschi S, Elzerman J M, Fujisawa T, Tarucha S and Kouwenhoven L P 2002 *Rev. Mod. Phys.* **75** 1–22
[26] Oosterkamp T H, Fujisawa T, van der Wiel W G, Ishibashi K, Hijman R V, Tarucha S and Kouwenhoven L P 1998 *Nature* **395** 873–6
[27] Harbusch D, Manus S, Tranitz H P, Wegscheider W and Ludwig S 2010 *Phys. Rev.* B **82** 195310
[28] Hayashi T T, Fujisawa H D C and Hirayam Y 2003 *Phys. Rev. Lett.* **91** 226804
[29] Li X Q and Arakawa Y 2001 *Phys. Rev.* A **63** 012302
[30] Gurvitz S A 1997 *Phys. Rev.* B **56** 15215–23
[31] Gardiner C W and Zoller P 2004 *Quantum Noise* 2nd edn (Berlin: Springer)
[32] Carmichael H J 2002 *Statistical Methods in Quantum Optics* (Berlin: Springer)
[33] Lambert N and Nori F 2008 *Phys. Rev.* B **78** 214302
[34] Li X Q, Luo J Y, Yang Y G, Cui P and Yan Y J 2005 *Phys. Rev.* B **71** 205304
[35] MacDonald D K C 1962 *Noise and Fluctuations: An Introduction* (New York: Wiley) chapter 2.2.1
[36] Engel H-A and Loss D 2004 *Phys. Rev. Lett.* **93** 136602
[37] Mozyrsky D, Fedichkin L, Gurvitz S A and Berman G P 2002 *Phys. Rev.* B **66** 161313
[38] Aguado R and Brandes T 2004 *Phys. Rev. Lett.* **92** 206601
[39] Luo J Y, Li X Q and Yan Y J 2007 *Phys. Rev.* B **76** 085325
[40] Jin J S, Li X Q, Luo M and Yan Y J 2011 *J. Appl. Phys.* **109** 053704
[41] Mu Y and Savage C M 1992 *Phys. Rev.* A **46** 5944–54
[42] Marthaler M 2009 *PhD Thesis* University Karlsruhe
[43] Harvey T J, Rodrigues D A and Armour A D 2008 *Phys. Rev.* B **78** 024513
[44] Emary C, Marcos D, Aguado R and Brandes T 2007 *Phys. Rev.* B **76** 161404
[45] Haroche S 1992 *Fundamental Systems in Quantum Optics* ed J Dalibard, J Raimond and J Zinn-Justin (New York: Elsevier) pp 767–940
[46] Jin J S, Zhang W-M, Li X-Q and Yan Y J 2011 arXiv:1105.0136
[47] André S, Jin P-Q, Brosco V, Cole J H, Romito A, Shnirman A and Schön G 2010 *Phys. Rev.* A **82** 053802
[48] Armour A D 2004 *Phys. Rev.* B **70** 165315
[49] Harvey T J, Rodrigues D A and Armour A D 2010 *Phys. Rev.* B **81** 104514
[50] Rodrigues D A 2009 *Phys. Rev. Lett.* **102** 067202